DOE/ET-53088-385 IFSR #385

Theory of High-n Toroidicity-Induced Shear Alfvén Eigenmode in Tokamaks

G.Y. Fu and *C.Z. Cheng**
Institute for Fusion Studies
The University of Texas at Austin
Austin, Texas 78712

July 1989

* *Princeton Plasma Physics Laboratory, Princeton University*
Princeton, NJ 08543

Theory of High-n Toroidicity-Induced Shear Alfvén Eigenmode in Tokamaks

G.Y. Fu
Center for Fusion Engineering and
Institute for Fusion Studies
The University of Texas at Austin
Austin, Texas 78712

and

C.Z. Cheng
Princeton Plasma Physics Laboratory
Princeton University
Princeton, NJ 08543

Abstract

High-n WKB-ballooning mode equation is employed to study toroidicity-induced shear Alfvén eigenmodes (TAE) in the $s - \alpha$ space, where $s = (r/q)(dq/dr)$ is the magnetic shear, and $\alpha = -(2Rq^2/B^2)(dp/dr)$ is the normalized pressure gradient for tokamak plasmas. In the ballooning mode first stability region, TAE modes are found to exist only for α less than some critical value α_c. We also find that these TAE modes reappear in the ballooning mode second stability region for bands of α values. The global envelope structures of these TAE modes are studied by WKB method and are found to be bounded radially if the local mode frequency has a maximum in radius.

I. Introduction

It is well known that shear Alfvén waves have continuous frequency spectrum in an inhomogeneous plasma.[1] In a toroidal plasma, toroidicity induces poloidal mode coupling which breaks up shear Alfvén continuum, and results in gaps in otherwise continuous spectrum. Recently, it has been found[2,3] that discrete modes can exist with frequencies inside these continuum gaps into a tokamak plasma. These modes are called toroidicity-induced shear Alfvén eigenmodes (TAE). These TAE modes have finite shear Alfvén frequencies and are marginally stable. More recently, it has been found[4-6] that TAE modes can be destabilized by super-Alfvénic fusion alpha particles in an ignited tokamak for both low-n and high-n modes, where n is the toroidal mode number.

In this work, we systematically study the high-n TAE modes in a tokamak plasma. In particular, we investigate the effects of curvature and pressure gradient on these modes. Previously,[2] high-n TAE modes were shown to exist in the absence of the finite pressure gradient effects. Our present work is motivated from the previous study of the low-n TAE modes.[7] In that work, it was found that finite plasma pressure would shift the eigenfrequency down toward the lower bound of the continuum gap. When the plasma beta is larger than a critical value ($2\% \sim 4\%$), the TAE mode frequency would move into the continuum, and the mode structure become singular. Since the low-n shear Alfvén equation is almost intractable analytically, we turn to high-n modes for which the WKB-ballooning mode representation[8-10] can be used to reduce the high-n two-dimensional wave equation to a simple second order differential equation along the field line, in the lowest order of $1/n \ll 1$.

Our main results are as follows. In the ballooning mode first stability region, the local eigenfrequency of the high-n TAE mode decreases as α increasing from zero, where α represents the product of magnetic field curvature and plasma pressure gradient, $\alpha =$

$-(2Rq^2/B^2)(dp/dr)$, R is the major radius, B is the toroidal magnetic field, q is the safety factor, P is the plasma thermal pressure, and r is the minor radius. For α values larger than a critical value $\alpha_c = \alpha_c(s)$, the TAE mode no longer exists. This critical α is derived analytically to be $\alpha_c = s^2/(1+s)$ for $s < 1$ and $\alpha_c = s + 1 - \sqrt{2s+1}$ for $s \gg 1$, where $s = (r/q)(dq/dr)$ is the magnetic shear. In the ballooning second stability region, we found that the TAE modes reappear for bands of α value. These α bands overlap at small shear $s \lesssim 0.1$. Finally, we found that the radial envelope for the TAE mode is bounded if the local frequency has a maximum in radius.

In Sec. II, we present the formulation of Alfvén wave equation and a brief discussion of the TAE modes. In Sec. III, the detailed numerical results and discussion are presented. Section IV provides an analytic derivation of the critical α values for the existence of the TAE modes in the ballooning mode first stability region. In Sec. V, the nonlocal envelope structures of the TAE modes are discussed. Finally, in Sec. VI, a summary and discussion are given.

II. High-n Shear Alfvén Wave Equation

In this section we derive the eigenmode equation for shear Alfvén waves with high toroidal mode number n for a toroidal plasma from the ideal MHD equations. Assuming that the perturbation quantities can be written as $\boldsymbol{\xi}(\mathbf{x},t) = \boldsymbol{\xi}(x)e^{-i\omega t}$, the linearized ideal MHD equations are given by

$$-i\omega\rho\mathbf{v} = \mathbf{j}\times\mathbf{B} + \mathbf{J}\times\delta\mathbf{B} - \nabla\delta p \tag{1}$$

and

$$\mathbf{E} + \mathbf{v}\times\mathbf{B} = 0 \tag{2}$$

where $\rho, \mathbf{B}, \mathbf{J}$ are the equilibrium density, magnetic field, and current density, respectively. Note that we have neglected the initial conditions in Eqs. (1) and (2), since we will be devoted to studying the eigenmode problem. The perturbed quantities are the electric field $\mathbf{E}$, the magnetic field $\delta\mathbf{B}$, the current density $\mathbf{j}$, the velocity $\mathbf{v}$, and the pressure δp. In terms of the electrostatic potential Φ and the vector potential $\mathbf{A}$, $\mathbf{E}$ and $\delta\mathbf{B}$ can be expressed as:

$$\mathbf{E} = -(\nabla\Phi - i\omega\mathbf{A}/c) \ , \tag{3}$$

and

$$\delta\mathbf{B} = \nabla \times \mathbf{A} \ . \tag{4}$$

Equations (1) and (2) are to be closed by the quasineutrality condition:

$$\nabla \cdot \mathbf{j} = 0 \ , \tag{5}$$

the adiabatic pressure law

$$-i\omega\delta p + \mathbf{v} \cdot \nabla P + \gamma_s P \nabla \cdot \mathbf{v} = 0 \ , \tag{6}$$

where γ_s is the ratio of specific heat, and the Ampere's law

$$\nabla^2\mathbf{A} = -\mathbf{j} \ . \tag{7}$$

The equilibrium force balance equation is given by

$$\mathbf{J} \times \mathbf{B} = \nabla P \ , \tag{8}$$

where P is the equilibrium pressure. From Eqs. (1) and (2), we obtain solutions for $\mathbf{v}$ and $\mathbf{j}$ given by

$$\mathbf{v} \ = \ \frac{\mathbf{E} \times \mathbf{B}}{B^2} - \frac{i(\delta\mathbf{B} \cdot \nabla P + \mathbf{B} \cdot \nabla\delta p)\mathbf{B}}{\omega\rho\, B^2} \ , \tag{9}$$

and

$$\mathbf{j}_\perp \;=\; [(\mathbf{J}\times\delta B - \nabla\delta p)\times\mathbf{B} - i\omega\rho\mathbf{E}_\perp]/B^2\ . \tag{10}$$

Now we consider perturbations with short wavelengths perpendicular to $\mathbf{B}$ in comparison with parallel wavelengths, $k_\parallel/k_\perp \ll 1$. By ignoring effects associated with the fast magnetosonic waves and the slow sound waves, we can neglect the $\nabla\cdot\mathbf{v}$ term in the adiabatic pressure law. Note that for a low-β, large aspect ratio tokamak, the $\nabla\cdot\mathbf{v}$ term is small when $\omega^2 \gg (c_s/qR)^2$ where c_s is the ion sound speed, and q the safety factor and R the major radius. With these assumptions, we have

$$\nabla_\perp(\delta p + \delta\mathbf{B}\cdot\mathbf{B}) \cong 0\ . \tag{11}$$

The quasineutrality condition, $\nabla\cdot\mathbf{j}=0$, then reduces to[11]

$$\mathbf{B}\cdot\nabla\frac{1}{B}\nabla^2\mathbf{A}\cdot\mathbf{B} - \frac{i\omega\rho}{B^2}\nabla_\perp^2\Phi + 2\,\frac{\boldsymbol{\kappa}\times\mathbf{B}}{B^2}\cdot\nabla_\perp\delta p = 0\ , \tag{12}$$

where $\boldsymbol{\kappa} = \mathbf{e}_b\cdot\nabla\mathbf{e}_b$ is the magnetic field curvature with $\mathbf{e}_b = \mathbf{B}/B$ being the unit vector along the magnetic field line. The equation of state, Eq. (6), becomes

$$-i\omega\delta p + \frac{\partial P}{\partial\psi}\frac{\partial\Phi}{\partial S} = 0 \tag{13}$$

where S and ψ are related to the equilibrium magnetic field by $\mathbf{B}=\nabla S\times\nabla\psi$. Combining Eq. (12) and Eq. (13), together with the condition of vanishing parallel electric field, we obtain the following linearized ideal ballooning equation for the shear Alfvén waves:

$$\mathbf{B}\cdot\nabla\left(\frac{\nabla_\perp^2}{B^2}\mathbf{B}\cdot\nabla\Phi\right) + \frac{\rho\omega^2}{B^2}\nabla_\perp^2\Phi - 2\frac{\boldsymbol{\kappa}\times\mathbf{B}}{B^2}\cdot\nabla_\perp\left(\frac{\mathbf{B}\times\nabla P}{B^2}\cdot\nabla\Phi\right) = 0\ . \tag{14}$$

Next, we consider perturbations with high toroidal mode number n and use $\delta = 1/n \approx \mathcal{O}(k_\parallel/k_\perp)$ as a small expansion parameter to develop an asymptotic solution of Eq. (14). Employing the high-n ballooning mode representation,[8-10] the perturbed quantities can be expressed as, e.g.,

$$\Phi(\psi,\theta,\zeta) = \sum_{\ell=-\infty}^{\infty}\hat{\Phi}(\psi,\theta-2\pi\ell,\zeta)\ , \tag{15}$$

where a (ψ, θ, ζ) flux coordinate system is adopted. With the ballooning mode formalism, the θ domain of $\widehat{\Phi}$ extends from $-\infty$ to ∞. If we let $S = \zeta - q(\psi)\theta$ in a toroidal system, then $2\pi\psi$ is the poloidal flux between the magnetic axis and a constant ψ surface. θ and ζ are the generalized poloidal and toroidal angles with a period of 2π, and the safety factor q is assumed to be a monotonic function of ψ only. In this coordinate system, $\mathbf{B}\cdot\nabla = j^{-1}\,(\partial/\partial\theta)_{S,\psi}$, where the Jacobian is $j = (\nabla\psi \times \nabla\theta \cdot \nabla\zeta)^{-1}$. It is clear that Eq. (14) is satisfied by the perturbed quantities over an infinite range in θ with no periodicity constraint. Then we express $\widehat{\Phi}$ by the WKB representation

$$\widehat{\Phi} = \phi(\psi, \theta, \delta)\exp[in\,\chi(S, \psi)]\ , \tag{16}$$

where χ describes the rapid cross-field variations and ϕ the slow variations along the field line on the equilibrium scale so that $\mathbf{B}\cdot\nabla\chi = 0$. For an axisymmetric toroidal system, χ is separable and can be expressed as

$$\chi = \left(S + \int \theta_k(\psi)dq\right)\ , \tag{17}$$

where θ_k is to be determined by a higher-order, radially nonlocal analysis. In the lowest order in δ, Eq. (14) then reduce to a second-order differential equation in θ for every ψ and θ_k. The final ideal ballooning equation is given[11]

$$j^{-1}\,\frac{\partial}{\partial\theta}\,\frac{|\nabla\chi|^2}{jB^2}\,\frac{\partial}{\partial\theta}\,\phi + \frac{\rho\omega^2}{B^2}\,|\nabla\chi|^2\phi + 2\,\frac{\partial P}{\partial\psi}\,\frac{\boldsymbol{\kappa}\cdot\mathbf{e}_b \times \nabla\chi}{B}\,\phi = 0\ . \tag{18}$$

For the purpose of analytical studies we consider an axisymmetric, large aspect ratio, low-β toroidal plasma with shifted circular magnetic surfaces.[12] Employing a (r, θ, ζ) coordinate system where r is the minor radius, θ is the poloidal angle, and ζ is the toroidal angle, the equilibrium magnetic field is given by $\mathbf{B} = B_0(1 - \hat{\varepsilon}\cos\theta)[\mathbf{e}_\zeta + (\hat{\varepsilon}/q)(1 + \Delta'\cos\theta)\mathbf{e}_\theta]$, $\hat{\varepsilon} = r/R$. After expanding to the first order in $\hat{\varepsilon}$, the high-n ideal ballooning equation, Eq. (18), reduces to

$$\frac{\partial}{\partial\theta}\left[G(\theta)\left(1 + h^2(\theta)\right)\right]\,\frac{\partial}{\partial\theta}\,\phi + \Omega^2 G(\theta)\,(1 + 2\hat{\varepsilon}\sigma\cos\theta) \times$$

$$\left(1+h^2(\theta)\right)\,\phi+\alpha(\cos\theta+h(\theta)\sin\theta)\,\phi=0\ , \tag{19}$$

where $h(\theta)=s(\theta-\theta_k)-\alpha\sin\theta$, $s=rq'/q$, $\Omega=\omega/\omega_A$, $\omega_A=v_A/qR$, $v_A^2=B_0^2/\rho$, $\alpha=2q^2R(dP/dr)/B_0^2$, and $G(\theta)=1+[2(\hat{\varepsilon}+\Delta')-\sigma\hat{\varepsilon}]\cos\theta$ with $\Delta'>0$ being the radial derivative of the Shafranov shift, σ is a quantity of order of unity which is related to the poloidal variation of the Jacobian, i.e., $j\propto 1+\sigma\hat{\varepsilon}\cos\theta$. Making the following transformation,

$$\phi\longrightarrow\frac{1}{\sqrt{G(\theta)\,(1+h^2(\theta))}}\,\phi\ ,$$

the ideal ballooning equation finally becomes

$$\frac{\partial^2}{\partial\theta^2}\,\phi+\left[\Omega^2-V(\theta)\right]\,\phi=0 \tag{20}$$

with $V(\theta)=F(\theta)-2\Omega^2\varepsilon\,\cos\theta$, where

$$F(\theta)=\frac{(s-\alpha\cos\theta)^2}{[1+h^2(\theta)]^2}-\frac{\alpha\cos\theta}{1+h^2(\theta)}\ , \tag{21}$$

where $\varepsilon=2\sigma\hat{\varepsilon}+(\hat{\varepsilon}-\sigma\hat{\varepsilon}+\Delta')/2\Omega^2$. At first, we note that as $\theta\to\infty$, $F\to 0$ and Eq. (20) becomes a Mathieu equation[13] which admits infinite pairs of real characteristic values Ω, these pairs of characteristic values define the gaps between the continuum bands. Physically, continuum gaps are caused by resonant reflection of waves by periodic potential. A similar example is the forbidden energy bands which appear in the energy spectrum of electrons in a periodic potential well of the crystal lattice.[14] For $\varepsilon\ll 1$, the continuum gaps located around $\Omega^2=\Omega_\ell^2=\ell^2/4$, $\ell=1,2,3,\ldots$, the size of the ℓth gap around Ω_ℓ^2 is order of $\mathcal{O}(\varepsilon^\ell)$. Here we consider the lowest gap ($\ell=1$) which is bounded by $\Omega^2=1/4(1\pm\varepsilon)$. Notice that for $\Omega\approx 1/2$, $\varepsilon=2(\hat{\varepsilon}+\Delta')$. For Ω inside the continuum gap around $\Omega^2=1/4$, $\phi\sim\exp(\pm\varepsilon_1\theta)$ asymptotically at large θ, where $\varepsilon_1\sim\mathcal{O}(\varepsilon)$.

It has been shown[2] that discrete eigenmode exists inside the continuum gap due to the contribution of $F(\theta)$ at finite θ. Figure 1 shows the mode structure of such an eigenmode with parameters of $\varepsilon=-0.2$, $s=0.8$, and $\alpha=\theta_k=0$. Physically, the $F(\theta)=s^2/(1+s^2\theta^2)$

term provides a potential barrier at $\theta = 0$ which can damp an otherwise growing travelling wave with frequency inside the continuum gap.

Previous work[2] has ignored the effect of finite pressure gradient α. Also only the lowest order local ballooning equation (18) has been considered. In the following sections, we will study the effects of arbitrary α value and will also consider the global solution of the ballooning equation (14).

III. Numerical Results and Discussion

We numerically integrate Eq. (20) using the shooting method which makes use of variable grid points. The boundary conditions for a bounded eigenmode is $\phi \to 0$ as $\theta \to \pm\infty$. For $\theta_k = 0$, the solution is either a pure even mode in θ or a pure odd mode due to the symmetry of Eq. (20). In this case, we integrate Eq. (20) from a large value of $\theta = \theta_m \gg 0$ to $\theta = 0$. The boundary conditions at $\theta = 0$ are $\phi'/\phi = 0$ for even mode and $\phi'/\phi = 0$ for odd modes, whereas at $\theta = \theta_m$, $\phi = 0$ and $\phi' = 1$. For $\theta_k \neq 0$ case, we integrate from $\theta = \theta_m$ to $\theta = -\theta_m$. The boundary condition at $\theta = -\theta_m$ is $\phi/\phi' = 0$. The value of θ_m is chosen such that the boundary conditions are satisfied and the solution is converged. Typically we have $\theta_m = 10\pi \sim 100\pi$, depending on the values of shear, α, and θ_k.

A. First ballooning bode stability region

Here we consider the effect of α on the TAE modes in the ideal ballooning mode first stability region. Figure 2 shows the eigenfrequency of the TAE mode as a function of α for $\epsilon = 0.2$ and $s = 0.8$, the dotted lines indicate the upper bound ($\Omega = \Omega_+$) and the lower bound ($\Omega = \Omega_-$) of the continuum gap, respectively. As α increases from zero, Ω decreases; for α value close to a critical value $\alpha_c = 0.34$, Ω approaches to the lower bound $\Omega = \Omega_-$ of the gap. The corresponding structures of the eigenmodes are shown in Fig. 3 for several α values. We observe that, as α approaching the critical value, the eigenfunction becomes

more and more extended. For $\alpha > \alpha_c$, we found that the TAE mode evolves into continuum and its eigenfunction is no longer L_2. Similar behaviors are also found for larger values of shear. Figure 4 shows the critical value α_c relative to the first ballooning mode stability boundary (dotted line). We found α_c scales as $\alpha_c \propto s^2$ for $s \ll 1$, and α_c approaches the ballooning mode first stability boundary for large shear.

The effects of α can be understood in terms of the potential $V(\theta) = F(\theta) - 2\Omega^2\varepsilon\cos\theta$. Figure 5 shows the potential $V(\theta)$ with $s = 0.8$, $\varepsilon = 0.2$ for a) $\alpha = 0$, and (b) $\alpha = \alpha_c = 0.34$. Recall that formation of a TAE mode inside the continuum gap is a result of the potential barrier at the center $\theta = 0$ due to the $F(\theta)$ term [see Fig. 5(a)]. From Fig. 5(b), however, we see that finite α can destroy this barrier at the center and therefore prevent the formation of the TAE mode.

B. Second ballooning mode stability region

Next we examine TAE modes in ideal ballooning mode second stability region. Both even modes and odd modes are investigated. Recall that the TAE modes no longer exist for α values larger than a critical value in the ballooning first stability region. Here, we found that the TAE modes reappear in the ballooning second stability region for bands of α values. Shown in Fig. 6 is (a) potential $V(\theta)$ (b) TAE mode with $\varepsilon = 0.2$, $s = 0.8$ and $\alpha = 2.9$ in the second α band, and (c) eigenfrequency as a function of α in the second α band. We observe that the potential barrier at $\theta = 0$ recovers for large α, at the same time a new potential peak appears away from the center. Accordingly, the TAE mode is localized between these two potential barriers. Making analogy with the quantum state of the Schrödinger equation with ϕ being particle wave function, $V(\theta)$ being potential and Ω^2 being the energy, the TAE mode can be seen as a bound state while the continuum mode as a travelling plane wave in the potential $V(\theta)$. Invoking the WKB argument, the bound state between these two potential barriers is possible only if a frequency within the gap is

compatible with the energy quantization condition. This constraint may give rise to bands of α value for which TAE modes can exist.

Notice that in Fig. 6(a), the off-cent potential peak locates approximately at the non-trivial zero point of $h(\theta) = 0$. For even larger $\alpha \gg s$, more potential peaks will appear since the number of zero points of $h(\theta) = 0$ is approximately equal to $\alpha/s\pi > 1$. Figure 7 shows the potential $V(\theta)$ for α values in a sequence of α bands with $s = 0.3$ and Fig. 8 shows the corresponding TAE modes. The eigenfrequencies of the TAE modes are shown in Fig. 9 for these three α bands. We observe that for $\alpha = 2.0$ in the second band, the TAE mode localized between the first peak at $\theta = 0$ and the second peak. Likewise, for $\alpha = 2.95$ in the third α band, the mode localized between the second peak and the third peak, and etc. We thus conjecture that there are infinite bands of α values and the TAE mode for the $(n+1)$th band is localized between the nth peak and the $(n+1)$th peak.

Before ending this section, we give an overview of the existence region of the TAE modes in $s - \alpha$ space. Figure 10 shows several α bands (shadowed region) in which the TAE modes exist; as a reference, the first stability boundary and the second stability boundary of the ideal ballooning modes are also shown (dotted lines) for $\theta_k = 0$. We observe that the first α band (in the first stability region) and second α band are nearly parallel to the stability boundaries for finite shear, and the slope of the higher bands decrease as α increases. For small values of shear $s \lesssim 0.1$, the α bands in the second stability region overlap. Finally, we point out that odd modes begin to appear for the third or higher bands.

IV. Analytic Theories

Here we will derive the critical α value for the existence of the TAE modes in the ballooning first stability region. First, we consider small shear $s < 1$. Following Cheng, Chen, and Chance,[2] we solve Eq. (20) by the two-scale, asymptotic matching method, using $\varepsilon \ll 1$ as a small parameter. Consider the TAE mode inside the lowest continuum gap, we

set $\Omega^2 \approx \frac{1}{4}$ and expand ϕ as

$$\phi = \phi_c \cos\left(\frac{\theta}{2}\right) + \phi_s \sin\left(\frac{\theta}{2}\right) , \tag{22}$$

where ϕ_c and ϕ_s represent the slow variation on scale $\theta \sim \mathcal{O}(1/\varepsilon)$. Average over the fast variation in $\cos(\theta/2)$ and $\sin(\theta/2)$, Eq. (20) then becomes

$$\frac{d^2\phi_c}{d\theta^2} + s^2 Y_+ \phi_c + \frac{d\phi_s}{d\theta} = 0 \tag{23}$$

and

$$\frac{d^2\phi_s}{d\theta^2} - s^2 Y_- \phi_s - \frac{d\phi_c}{d\theta} = 0 , \tag{24}$$

$$Y_\pm = \frac{\overline{\Omega}_\pm^2}{s^2} + \frac{a_\pm}{1+s^2\theta^2} + \frac{b_\pm}{(1+s^2\theta^2)^2} . \tag{25}$$

Here $\overline{\Omega}_\pm^2 = \pm\left[\Omega^2(1\pm\varepsilon) - \frac{1}{4}\right] > 0$, $a_\pm = \frac{1}{2}\alpha/s^2$ and $b_\pm = \pm\left(s^2 + \frac{1}{2}\alpha^2 \pm s\alpha\right)/s^2$. If we let $y = s\theta$, then Eqs. (23) and (24) can be combined to give

$$s^2\left(\frac{d}{dy}\frac{1}{Y_-}\frac{d}{dy} - 1\right)\left(\frac{d^2}{dy^2} + Y_+\right)\phi_c + \frac{d}{dy}\frac{1}{Y_-}\frac{d}{dy}\phi_c = 0 . \tag{26}$$

Notice that $\overline{\Omega}_\pm^2 \sim \mathcal{O}(\varepsilon)$, we can then solve Eq. (26) by the asymptotic matching method. We divide y in three regions: (i) $y \sim \mathcal{O}(1)$, (ii) $y \sim \mathcal{O}(1/\sqrt{\varepsilon})$ and (iii) $y \sim \mathcal{O}(1/\varepsilon)$. Then in these regions, Eq. (26) reduces to:

$$s^2\left[\frac{d}{dy}\frac{1}{\frac{a_-}{1+y^2} + \frac{b_-}{(1+y^2)^2}}\frac{d}{dy} - 1\right]\left[\frac{d^2}{dy^2} + \frac{a_+}{1+y^2} + \frac{b_+}{1+y^2)^2}\right]\phi_c^1$$
$$+ \frac{d}{dy}\frac{1}{\frac{a_-}{1+y^2} + \frac{b_-}{(1+y^2)^2}}\frac{d}{dy}\phi_c^1 = 0 \tag{27}$$

in the region (i), to

$$\frac{d}{dy}\frac{1}{\frac{\overline{\Omega}_-^2}{s^2} + \frac{a_-}{1+y^2}}\frac{d}{dy}\phi_c^2 = 0 \tag{28}$$

in the region (ii), and to

$$\frac{\overline{\Omega}_-^2}{s^2}\frac{d^2}{dy^2}\phi_c^3 - \overline{\Omega}_+^2\phi_c^3 = 0 \tag{29}$$

in the region (iii).

The solutions of Eq. (28) and (29) are given by the following:

$$\phi_c^2 = c_1 \left[\frac{\overline{\Omega}_-^2}{s^2} y - \frac{a_-}{y} + c_2 \right] \tag{30}$$

and

$$\phi_c^3 = c_3 \exp\left(-\frac{\overline{\Omega}_+ \overline{\Omega}_-}{s} y \right) , \tag{31}$$

where c_1, c_2 and c_3 are integration constants. To solve Eq. (27), we expand ϕ_c^1 using $s^2 < 1$ as a small parameter,

$$\phi_c^1 = \phi_0 + s^2 \phi_1 . \tag{32}$$

Then the even parity solution can be obtained straightforwardly with

$$\phi_0 = 1 \tag{33}$$

and

$$\begin{aligned} \phi_1 = & -\frac{a_+}{1+y^2} - \frac{b_+}{(1+y^2)^2} - \frac{a_- b_-}{4} \frac{1}{1+y^2} + \left(a_+ + \frac{b_+}{2} \right) \frac{a_-}{2} \left(tg^{-1} y \right)^2 \\ & + \left(a_+ + \frac{b_+}{2} \right) \frac{b_-}{4} \left(tg^{-1} y + \frac{y}{1+y^2} \right)^2 . \end{aligned} \tag{34}$$

After matching ϕ_c^1, ϕ_c^2 and ϕ_c^3, we obtain the following dispersion relation for $s < 1$

$$\frac{\overline{\Omega}_+}{\overline{\Omega}_-} = \frac{\pi}{4} s \left[1 - \frac{\alpha(1+s)}{s^2} \right] \tag{35}$$

or more explicitly:

$$\Omega^2 = \frac{1}{4} \left[1 + \varepsilon \frac{1-\Lambda}{1+\Lambda} \right]^{-1} \tag{36}$$

with $\Lambda = \frac{\pi^2}{16} s^2 \left(1 - \alpha(1+s)/s^2 \right)$. The analytic result of Eq. (36) shows that as α increases, the eigenfrequency Ω decreases. When $\alpha = s^2/(1+s)$, Ω hits the lower bound of the

continuum gap (i.e., $\Omega^2 = \frac{1}{4}(1+\varepsilon)^{-1}$). Thus we obtain the critical α value for which TAE modes no longer exists:

$$\alpha_c = s^2/(1+s) \ . \tag{37}$$

Figure 11(a) compares analytic α_c with the numerical calculation. We observe that the agreement is very good. Similar dispersion like Eq. (35) has been independently derived by Chen *et al.*[6]

Next, we consider the case of large shear $s \gg 1$. For this case, the two-scale analysis is no longer applicable. Instead, the variational method[15] may be used. Equation (20) can be rewritten into a quadratic form:

$$I = \int_{-\infty}^{\infty} d\theta \left\{ \left(\frac{d\phi}{d\theta}\right)^2 - \left[\Omega^2(1+2\varepsilon\cos\theta) - F(\theta)\right]\phi^2 \right\} = 0 \ . \tag{38}$$

We take the following trial function with parameters λ_1 and λ_2 to be determined:

$$\phi = \phi_t = \left(\cos(\theta/2) + \lambda_1 \sin\left|\frac{\theta}{2}\right|\right) e^{-\lambda_2|\theta|/2} \ , \tag{39}$$

where $\lambda_2 > 0$. Notice that for $s - \alpha \gg 1$, $F(\theta)$ peaks at $\theta = 0$, so we can approximate $F(\theta)$ as

$$F(\theta) = \frac{(s-\alpha)^2}{\left(1+(s-\alpha)^2\theta^2\right)^2} - \frac{\alpha}{1+(s-\alpha)^2\theta^2} \ . \tag{40}$$

Then $I = I(\lambda_1, \lambda_2)$ can be evaluated straightforwardly to be

$$\begin{aligned} I(\lambda_1,\lambda_2) \ = \ & \frac{\lambda_1^2\overline{\Omega}_-^2 - \overline{\Omega}_+^2}{\lambda_2} - \frac{\left(2\Omega^2+\frac{1}{2}\right)\lambda_1}{1+\lambda_2^2} + \frac{(1-\lambda_1^2)\lambda_2 + 2\lambda_1}{4+\lambda_2^2}\Omega^2\varepsilon \\ & + A(\lambda_1,\lambda_2)\lambda_2 + \frac{\pi}{2}(s-\alpha)\left[1 - \frac{2\alpha}{(s-\alpha)^2}\right] \ , \end{aligned} \tag{41}$$

where

$$A(\lambda_1,\lambda_2) = \frac{1}{4}(1+\lambda_1^2) - \frac{\frac{1}{4}(\lambda_1^2-\lambda_2^2) - \frac{1}{2} + \left(\lambda_1\lambda_2+\frac{1}{2}\right)^2 + \Omega^2(1-\lambda_2^2+2\varepsilon+2\varepsilon\lambda_1^2)}{1+\lambda_1^2} \ . \tag{42}$$

Recall that $\overline{\Omega}_{\pm}^2 \sim \mathcal{O}(\varepsilon)$. According to the asymptotic behavior of ϕ at large θ given in Eq. (31), we order $\lambda_1 \sim \mathcal{O}(1)$ and $\lambda_2 \sim \mathcal{O}(\varepsilon)$. Keeping only the lowest order terms, Eq. (41) then reduces to

$$I(\lambda_1, \lambda_2) = \frac{\lambda_1^2 \overline{\Omega}_-^2 - \overline{\Omega}_+^2}{\lambda_2} - \lambda_1 + \frac{\pi}{2}(s-\alpha)\left(1 - \frac{2\alpha}{(s-\alpha)^2}\right) . \tag{43}$$

Now $\frac{\partial I}{\partial \lambda_1} = 0$ and $\frac{\partial I}{\partial \lambda_2} = 0$ gives

$$\lambda_2 = 2\lambda_1 \overline{\Omega}_-^2 \tag{44}$$

$$\lambda_1^2 = \overline{\Omega}_+^2 / \overline{\Omega}_-^2 . \tag{45}$$

Since we require $\lambda_2 > 0$, we have $\lambda_1 = \overline{\Omega}_+ / \overline{\Omega}_-$ and $\lambda_2 = 2\overline{\Omega}_+ \overline{\Omega}_-$. Thus, we obtain a dispersion relation from $I(\lambda_1, \lambda_2) = 0$

$$\frac{\overline{\Omega}_+}{\overline{\Omega}_-} = \frac{\pi}{2}(s-\alpha)\left[1 - \frac{2\alpha}{(s-\alpha)^2}\right] . \tag{46}$$

The critical α value for $s \gg 1$ is then given by

$$\alpha_c = s + 1 - \sqrt{2s+1} . \tag{47}$$

Figure 11(b) compares the analytic result, Eq. (47), with the numerical result. The agreement is very good.

V. Nonlocal Theory

In the preceding sections, we only consider the local theory of high-n TAE modes, which determines local frequency Ω or $\omega = \omega(\psi, \theta_k)$ as a function of flux surface and radial wave number θ_k. Recall that the local ballooning mode equation given by Eq. (18) is obtained by expanding the high-n ideal MHD equation to the lowest order of small parameter $\delta = 1/n$. This lowest order equation only determines the local fast variation along ψ, and θ. In order

to determine the slow variation of the radial envelope for these local modes, i.e., the radial dependence of ϕ on ψ, we need to expand high-n MHD equation to higher order.[8] To obtain radially bounded solutions, the following WKB quantization condition[11] must be satisfied,

$$\oint \theta_k(\psi,\omega)\, dq = \left(\ell + \frac{1}{2}\right)\pi \ , \tag{48}$$

where ℓ is zero or positive integer, and we have assumed that the constant ω curves in ψ, θ_k space are closed.

Now we consider the dependence of local frequency ω as a function of θ_k. Since Eq. (20) has a symmetry in θ (due to the up-down symmetry of tokamak geometry considered in this paper), we have

$$\omega(\psi,-\theta_k) \ = \ \omega(\psi,\theta_k) \ . \tag{49}$$

We also have the obvious periodicity constraint:

$$\omega(\psi,\theta_k+2\pi) \ = \ \omega(\psi,\theta_k) \ . \tag{50}$$

Figures 12(a) and (b) show typical variations of the normalized frequencies $\Omega = \omega/\omega_A$ as a function of θ_k in the ballooning first stability region for (a) $s = 0.8$, $\alpha = 0$, $\varepsilon = 0.2$, and (b) $\alpha = 0.15$, $s = 0.8$ and $\varepsilon = 0.2$. We observe that in both cases

$$\left.\frac{\partial\Omega}{\partial\theta_k}\right|_{\theta_k=0} = 0 \qquad \text{and} \qquad \left.\frac{\partial^2\Omega}{\partial\theta_k^2}\right|_{\theta_k=0} < 0 \ . \tag{51}$$

Thus, whether the constant ω contours are closed or open in the (ψ,θ_k) space depends on the radial variations of the local frequency $\omega(\psi,\theta_k)$. For realistic tokamak equilibrium, the shear Alfvén frequency $\omega_A = v_A/qR$ is nonuniform. Figure 13(a) shows a possible ω profile as a function of flux surface which possesses a local maximum with $\theta_k = 0$. The dotted lines in Fig. 13(a) represent the upper bound and the lower bound of the continuum gap. The corresponding ω contour is shown schematically in Fig. 13(b). We observe that the contour is closed around the local maximum $\psi = \psi_0$. In this case, the global frequency for

the TAE mode is determined by the quantization condition given by Eq. (48) and the mode is bounded between the two turning points. On the other hand, Figs. 14(a) and (b) show a case in which $\omega(\psi, \theta_k)$ does not have a local maximum in ψ and the constant ω-contours are open. Then, the TAE mode structure can not be bounded and it could be damped by phase mixing associated with the shear Alfvén continuum. We thus conclude that damping-free radially bounded TAE modes exist only if the local mode frequency has a maximum in radius.

VI. Conclusion

In this paper, high-n toroidicity-induced Alfvén eigenmodes are studied systematically for arbitrary shear and pressure gradient. We found that discrete local TAE modes exist with frequencies inside the continuum gap only for bands of α value. In particular, the local TAE modes exist only for α less than some critical value $\alpha_c = \alpha_c(s)$ in the ballooning mode first stability region. The global envelope for these local modes can be determined by the higher-order equation. The envelope is bounded radially if the local TAE mode frequency has a maximum in radius. Otherwise, the envelope is not localized and Alfvén resonant absorption associated with shear Alfvén continuum could occur. Thus, whether a damping-free discrete TAE mode exists depends on the realistic tokamak profiles, in particular, the shear Alfvén frequency $\omega_A = v_A/qR$ profile and pressure profile.

Acknowledgments

One of the authors (GYF) gratefully acknowledges Dr. Liu Chen for useful discussions. This work was supported by the U.S. Department of Energy under contract DE-AC02-76-CHO-3073 at Princeton Plasma Physics Laboratory and contract DE-FG05-80ET-53088 at the Institute for Fusion Studies, and by the Texas Advanced Technology Program and the Texas Atomic Energy Research Foundation.

References

1. Z. Sedlacek, J. Plasma Phys. **5**, 239 (1971); and E.M. Barston, Ann. Phys. (N.Y.), **29**, 282 (1964).

2. C.Z. Cheng, L. Chen, and M.S. Chance, Ann. Phys. (NY) 161, 21(1984)

3. C.Z. Cheng and M.S. Chance, Phys. Fluids **29**, 3695 (1986).

4. G.Y. Fu, Ph.D. Thesis, The University of Texas at Austin, Institute for Fusion Studies Report No. 325 (1988)

5. G.Y. Fu, J.W. Van Dam, M.N. Rosenbluth, D.W. Ross, Y.Z. Zhang, H.L. Berk, S.M. Mahajan, C.Z. Cheng, R.L. Miller, X.H. Wang, A. Bhattacharjee, M.E. Mauel, and B. Breizman, in *Plasma Physics and Controlled Nuclear Fusion Research 1988,* Proceedings of the 12th International Conference (Nice, France, October 12-19, 1988), Paper IAEA-CN-50/D-4-11, to be published.

6. Liu Chen, Princeton Plasma Physics Laboratory Report, PPPL-2597 (1989).

7. C.Z. Cheng, G.Y. Fu, and J.W. Van Dam, Princeton Plasma Physics Laboratory Report No. 2585 (Jan., 1989), to be published in the Proceedings of the Joint Varenna-Lausanne International Workshop on Theory of Fusion Plasmas (October 3-7, 1988, Chexbres, Switzerland).

8. A.H. Glasser, in Finite Beta Theory Workshop (Proc. Varenna, 1977) (B. Coppi, W. Sadowski, Eds.) U.S. Dept. of Energy, CONF-7709167, p. 552, 1977.

9. Y.C. Lee and J.W. Van Dam, in Finite Beta Theory Workshop (Proc. Varenna, 1977) (B. Coppi, W. Sadowski, eds.), U.S. Dept. of Energy, CONF-7709167, p. 93, 1977.

10. J.W. Connor, R.J. Hastie, and J.B. Taylor, Proc. R. Soc. London, Ser **A 365**, 1 (1979).

11. M.S. Chance, R.L. Dewar, E.A. Frieman, A.H. Glasser, J.M. Greene, R.C. Grimm, S.C. Jardin, J.L. Johnson, J. Manickam, M. Okabayashi, A.M.M. Todd, in *Plasma Physics and Controlled Thermonuclear Fusion Research* (IAEA, Vienna, 1978), Vol. I, p. 677.

12. J.W. Connor, R. Hastie, and J.B. Taylor, Phys. Rev. Lett. **40**, 396 (1978).

13. M. Abramowitz and I.A. Stegun, *Handbook of Mathematical Function,* U.S. Dept. of Commerce, National Bureau of Standards, AMS55 (1964).

14. C. Kittell, *Introduction to Solid State Physics,* (Wiley, NY, 1976).

15. L.Chen, A. Bondeson, and M.S. Chance, Nucl. Fusion **27**, 1918 (1987).

Figure Captions

1. TAE mode with parameters of $s = 0.8$, $\alpha = 0$, $\varepsilon = 0.2$, and $\theta_k = 0$.

2. Eigenfrequency Ω of TAE mode as a function of α for $\varepsilon = 0.2$ and $s = 0.8$. The dotted lines indicate the upper bound ($\Omega = \Omega_+$) and the lower bound ($\Omega = \Omega_-$) of the continuum gap.

3. TAE mode structure for a sequence of α values with $\varepsilon = 2.0$, $\theta_k = 0$, and $s = 0.8$. (a) $\alpha = 0.15$ (b) $\alpha = 0.25$ (c) $\alpha = 0.321$.

4. Critical α_c (solid line) relative to the ballooning mode first stability boundary (dotted line).

5. Potential $v(\theta)$: (a) $\alpha = 0$, (b) $\alpha = 0.34$ with $\varepsilon = 0.2$, $\theta_k = 0$, and $s = 0.8$.

6. (a) potential $v(\theta)$ and (b) TAE modes for $\alpha = 2.9$; (c) eigenfrequency for second α band with $\varepsilon = 0.2$, $\theta_k = 0$, and $s = 0.8$.

7. Potential $v(\theta)$ for a sequence of α value with $\varepsilon = 0.2$ and $s = 0.3$: (a) $\alpha = 2.0$, (b) $\alpha = 2.95$, and (c) $\alpha = 4.5$.

8. TAE modes corresponding to parameters of Fig. 7.

9. Eigenfrequency as a function of α in the ballooning second stability region with $\varepsilon = 0.2$ and $s = 0.3$.

10. Existence region for TAE modes for the parameters of $\varepsilon = 0.2$ and $\theta_k = 0$; the dotted lines show the ballooning stability boundaries.

11. Analytic critical α_c (dotted line) and the numerical α_c (solid line) as a function of shear s for the parameter of $\varepsilon = 0.2$ and $\theta_k = 0$: (a) $s < 1$, (b) $s \gg 1$.

12. Frequency Ω as a function of θ_k for (a) $s = 0.8$, $\alpha = 0.0$ and $\varepsilon = 0.2$, and (b) $S = 0.8$, $\alpha = 0.15$, and $\varepsilon = 0.2$.

13. (a) $\omega(\psi, \theta_k)$ profile as a function of ψ at $\theta_k = 0$, (b) ω contour in (ψ, θ_k) space.

14. (a) $\omega(\psi, \theta_k)$ profile as a function of ψ at $\theta_k = 0$, (b) ω contour in (ψ, θ_k) space.

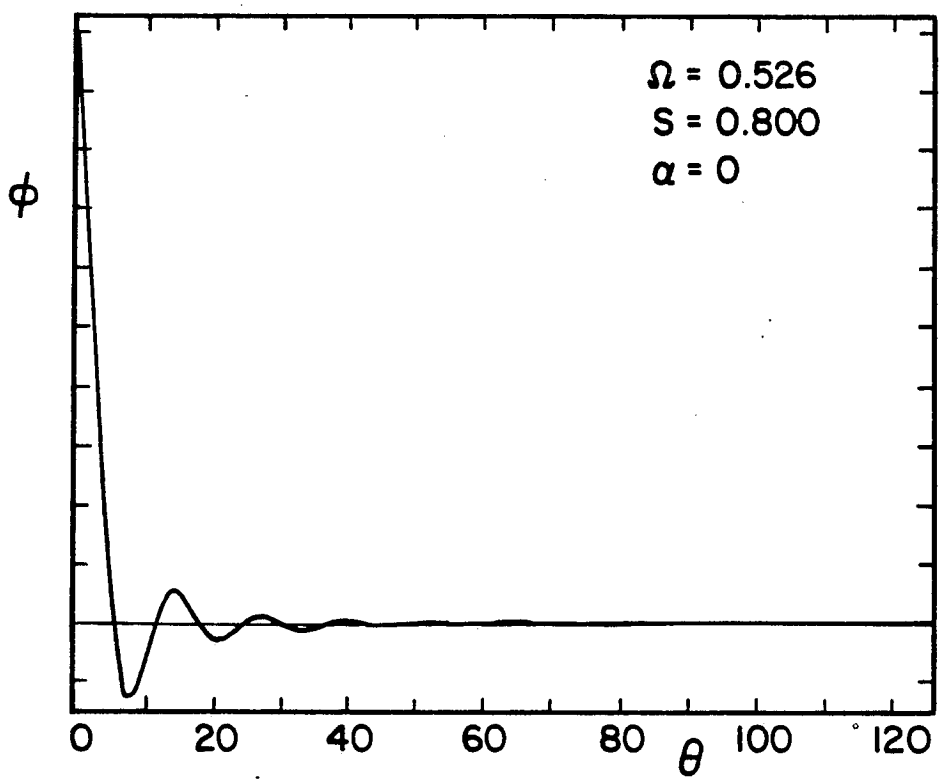

Fig. 1

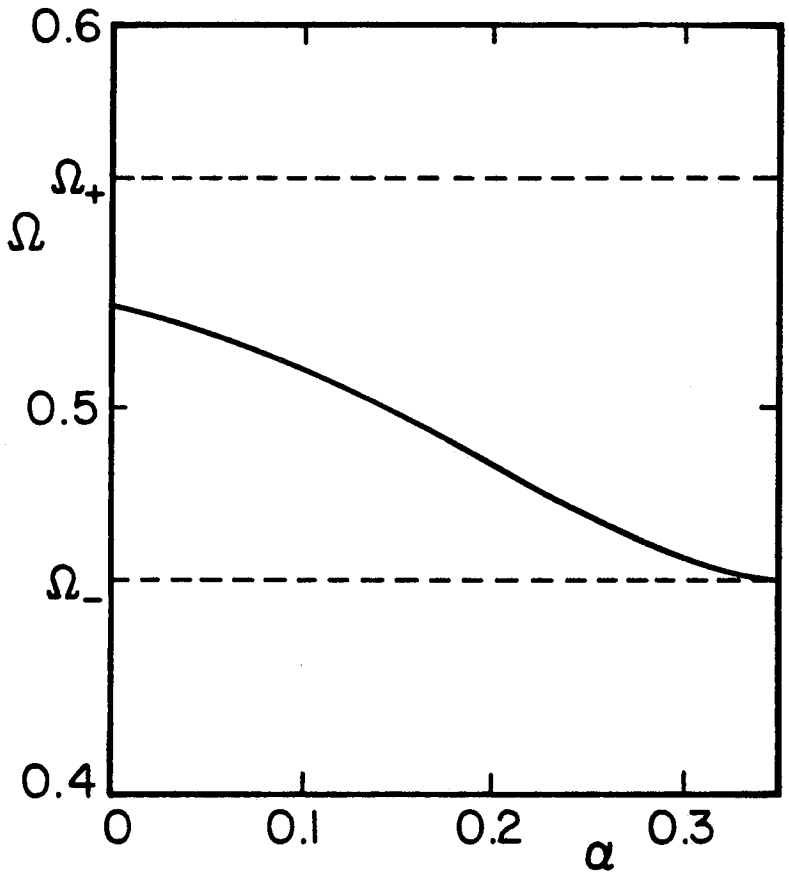

Fig. 2

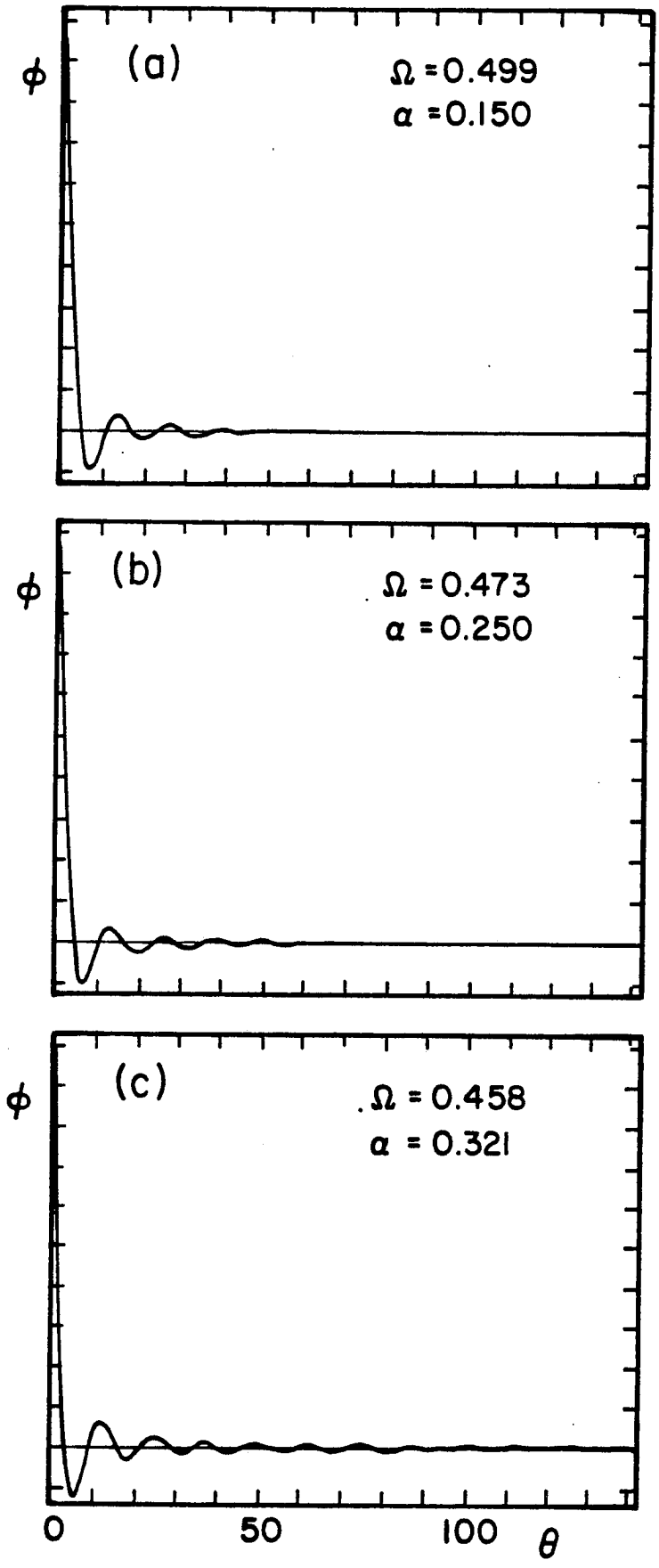

Fig. 3

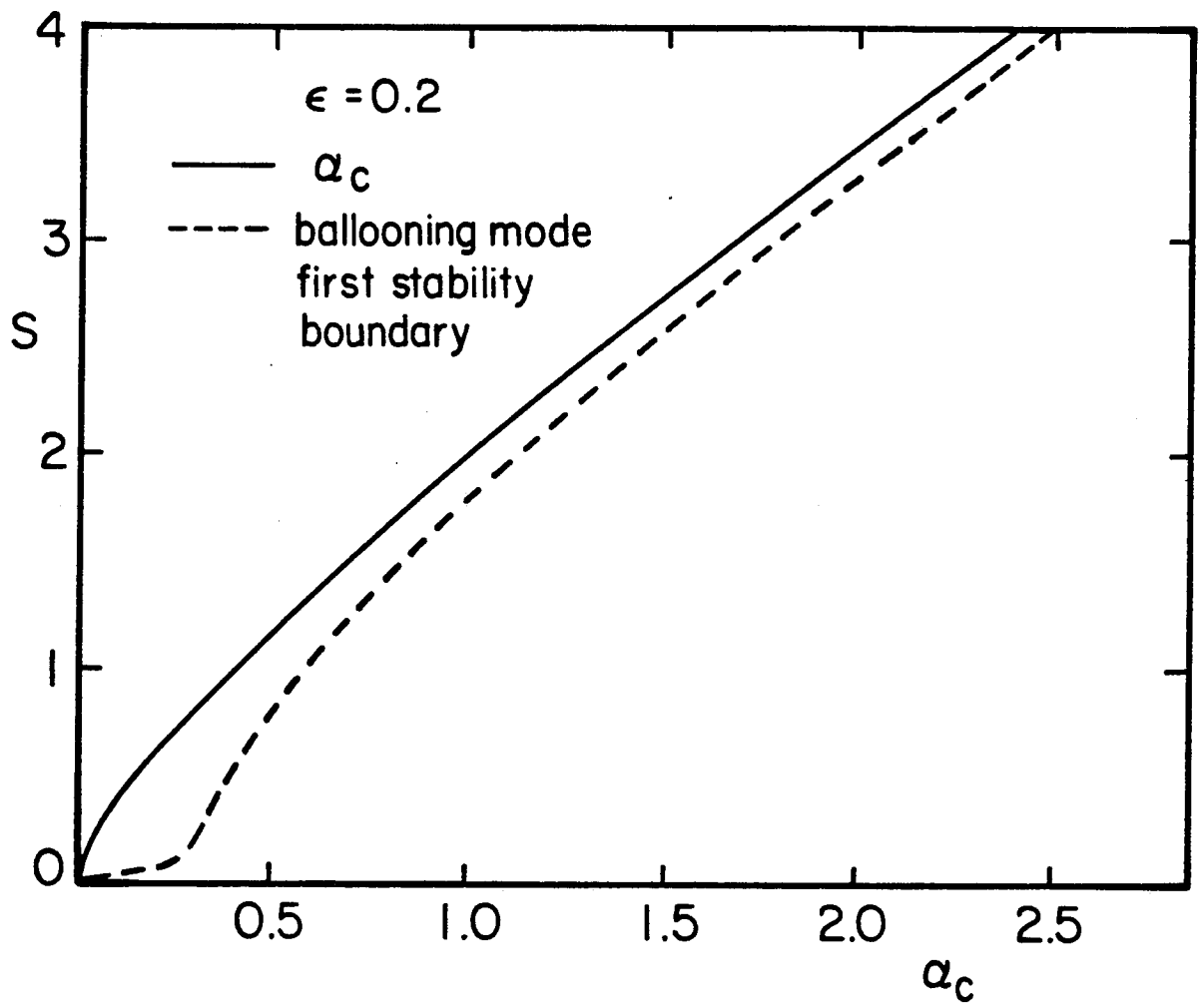
4
3
2
1
0
S
ϵ = 0.2
α_c
ballooning mode
first stability
boundary
0.5
1.0
1.5
2.0
2.5
α_c

Fig. 4

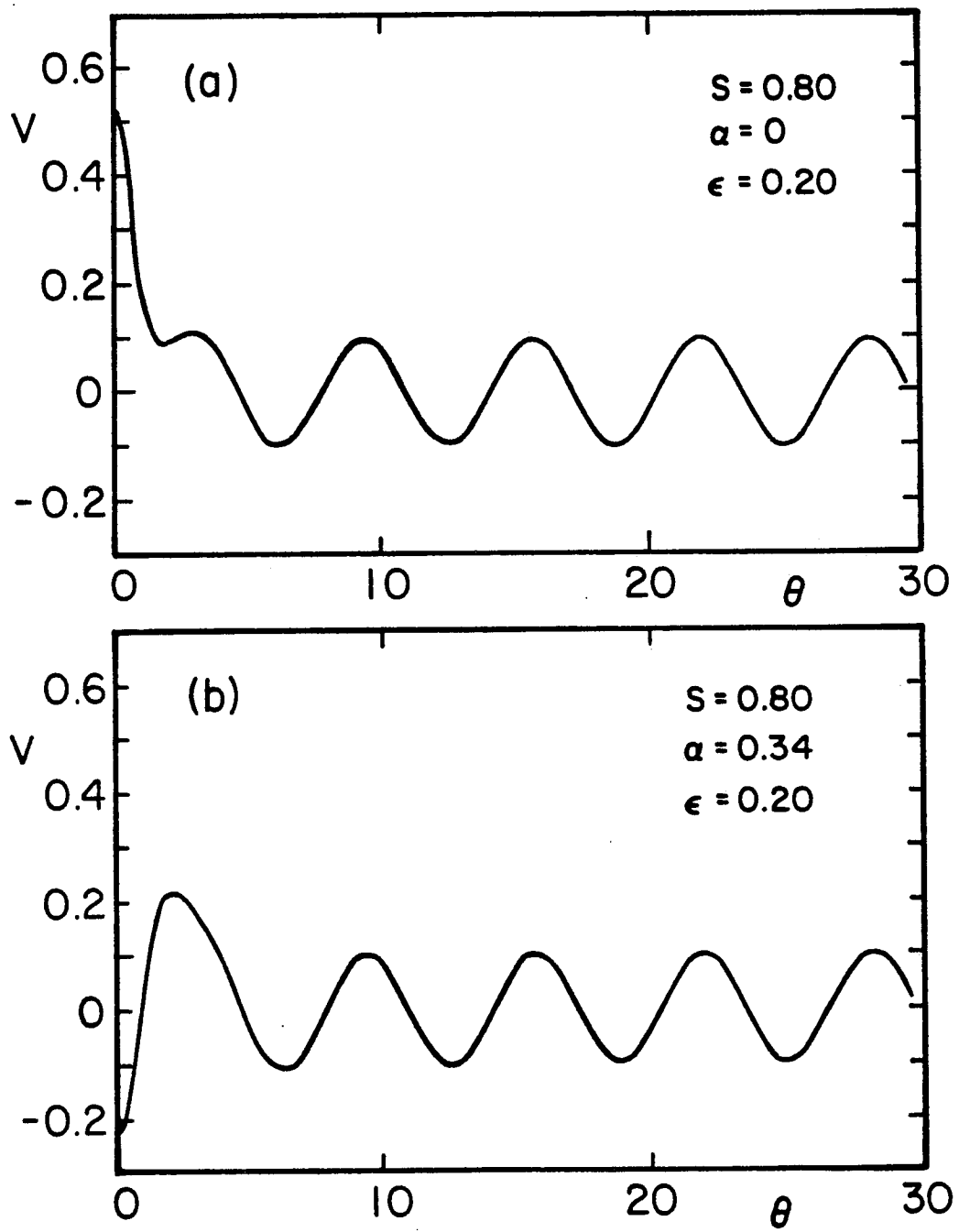
(a)
S = 0.80
α = 0
ϵ = 0.20
V
0.6
0.4
0.2
0
-0.2
0
10
20
θ
30
(b)
S = 0.80
α = 0.34
ϵ = 0.20
V
0.6
0.4
0.2
0
-0.2
0
10
20
θ
30

Fig. 5

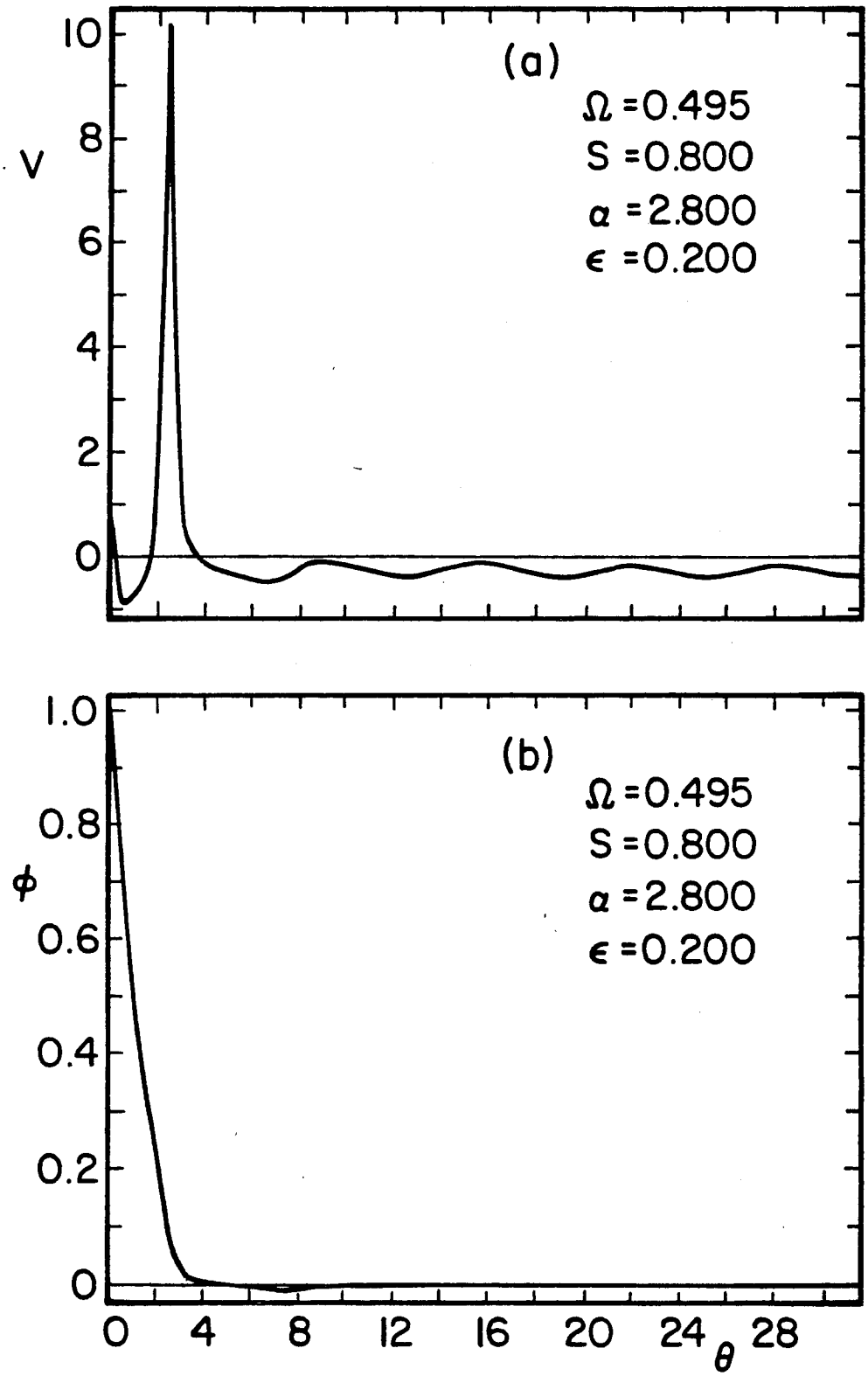
(a)
Ω =0.495
S =0.800
α =2.800
ϵ =0.200
V
10
8
6
4
2
0
(b)
Ω =0.495
S =0.800
α =2.800
ϵ =0.200
φ
1.0
0.8
0.6
0.4
0.2
0
0
4
8
12
16
20
24
28
θ

Fig. 6(a)-(b)

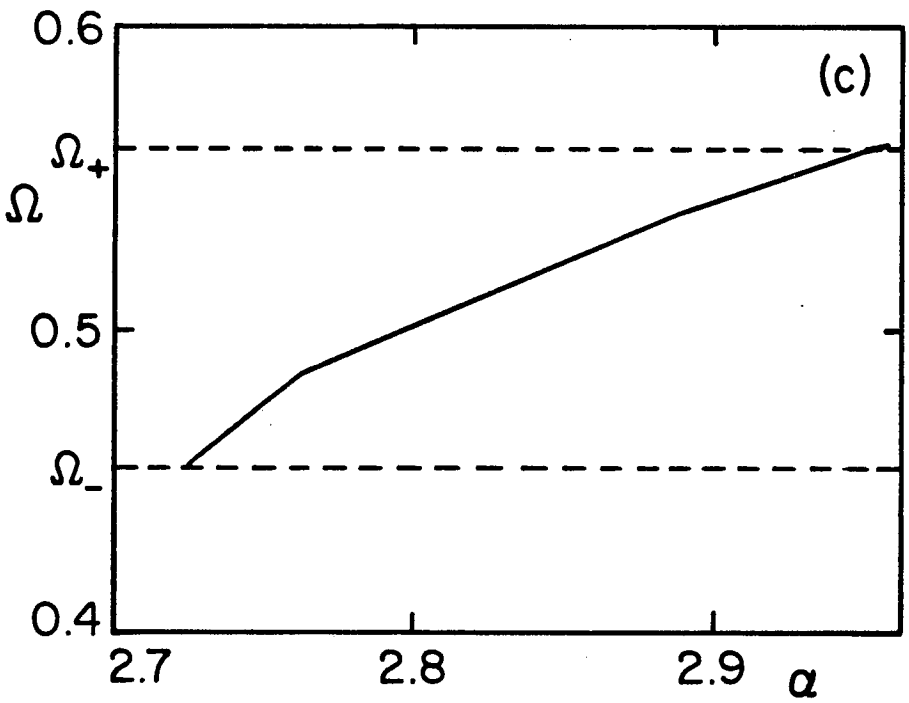

Fig. 6(c)

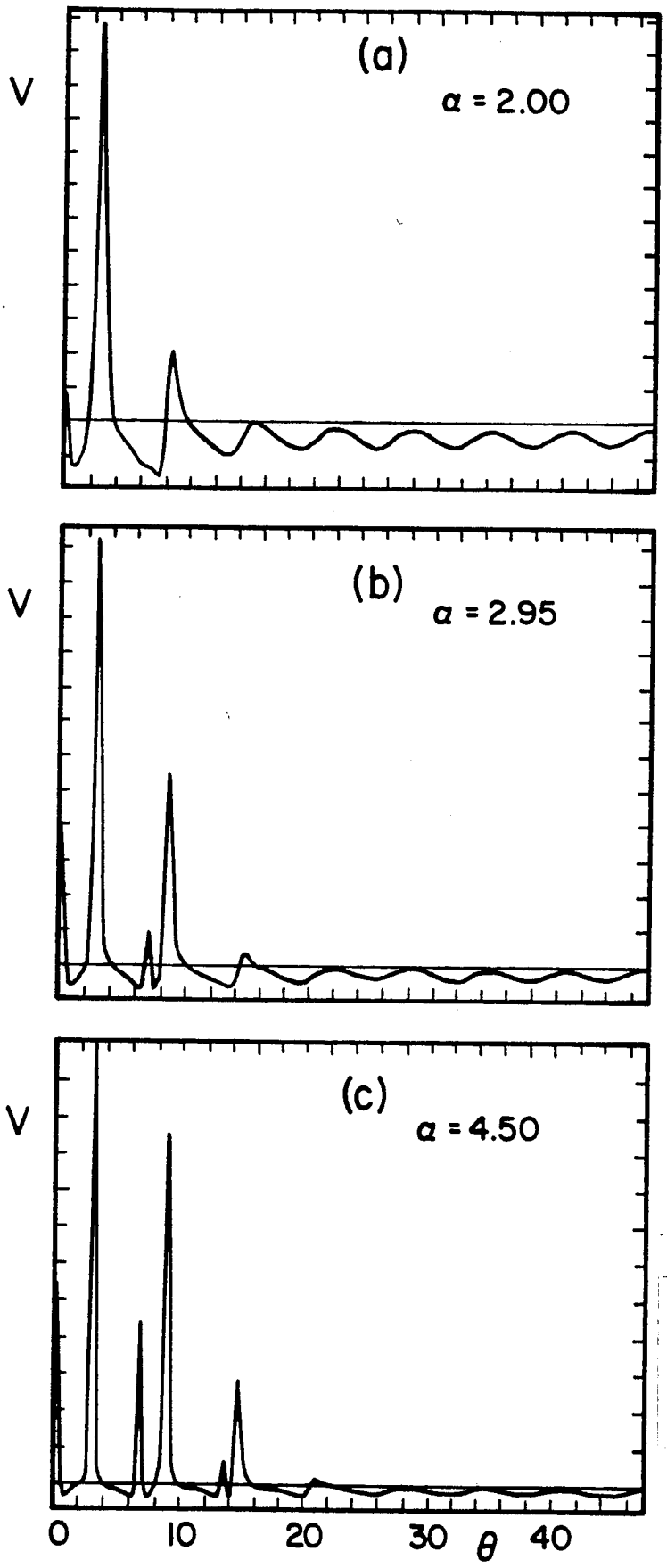

Fig. 7

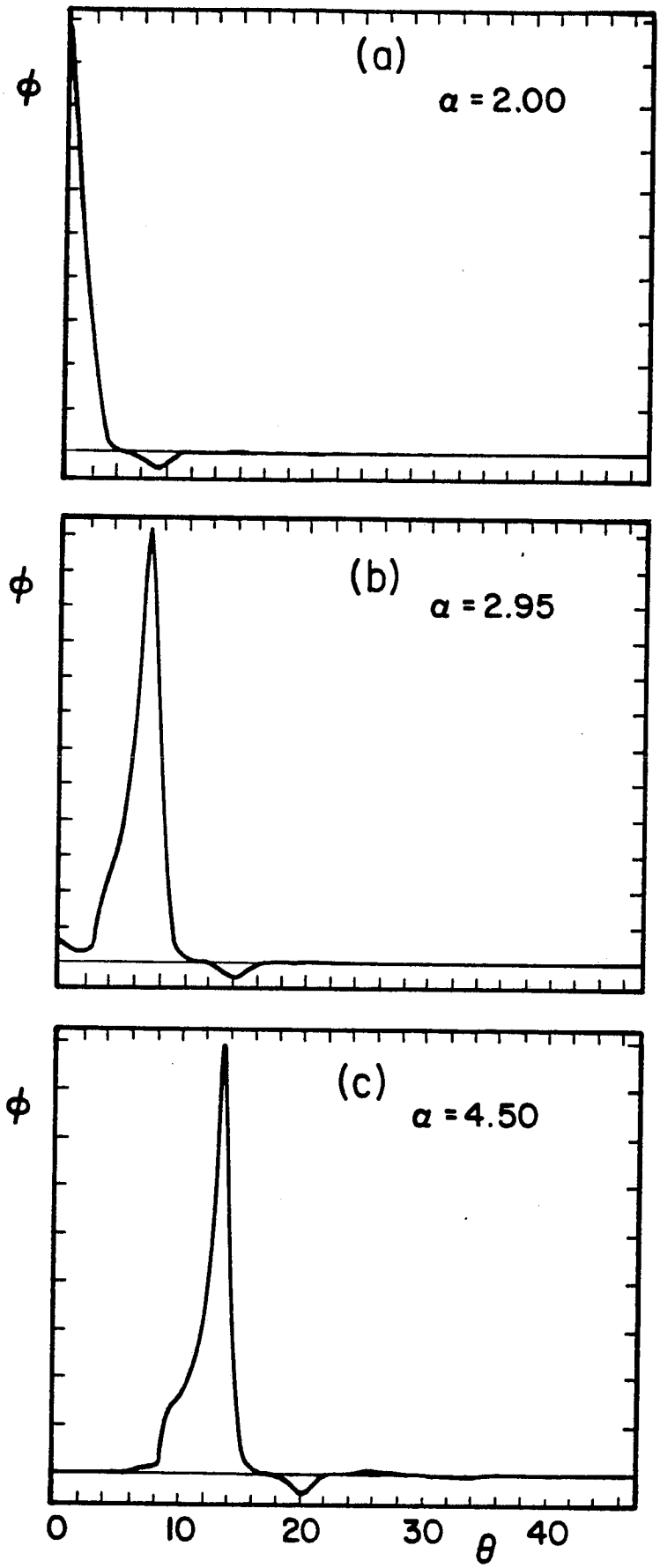

Fig. 8

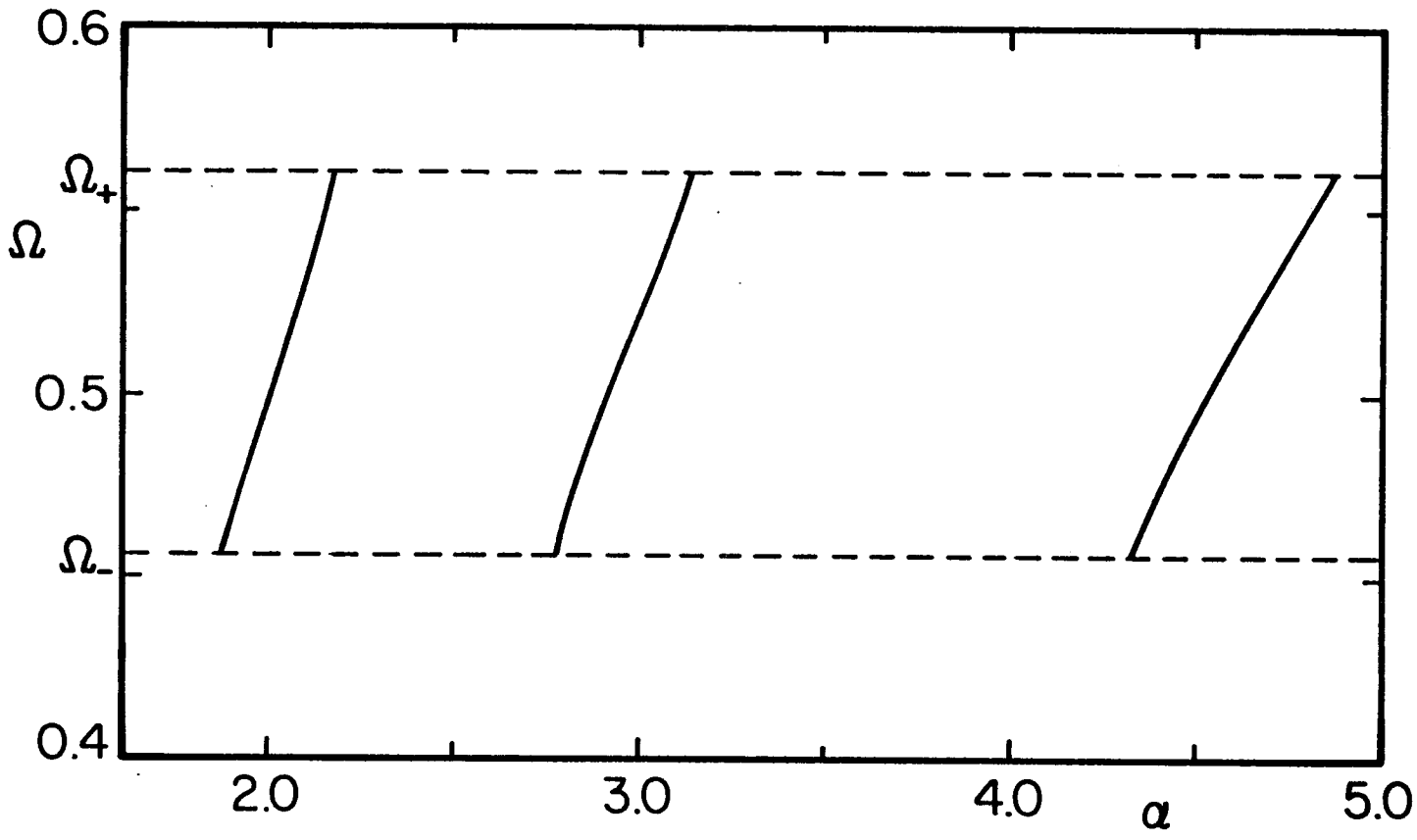

Fig. 9

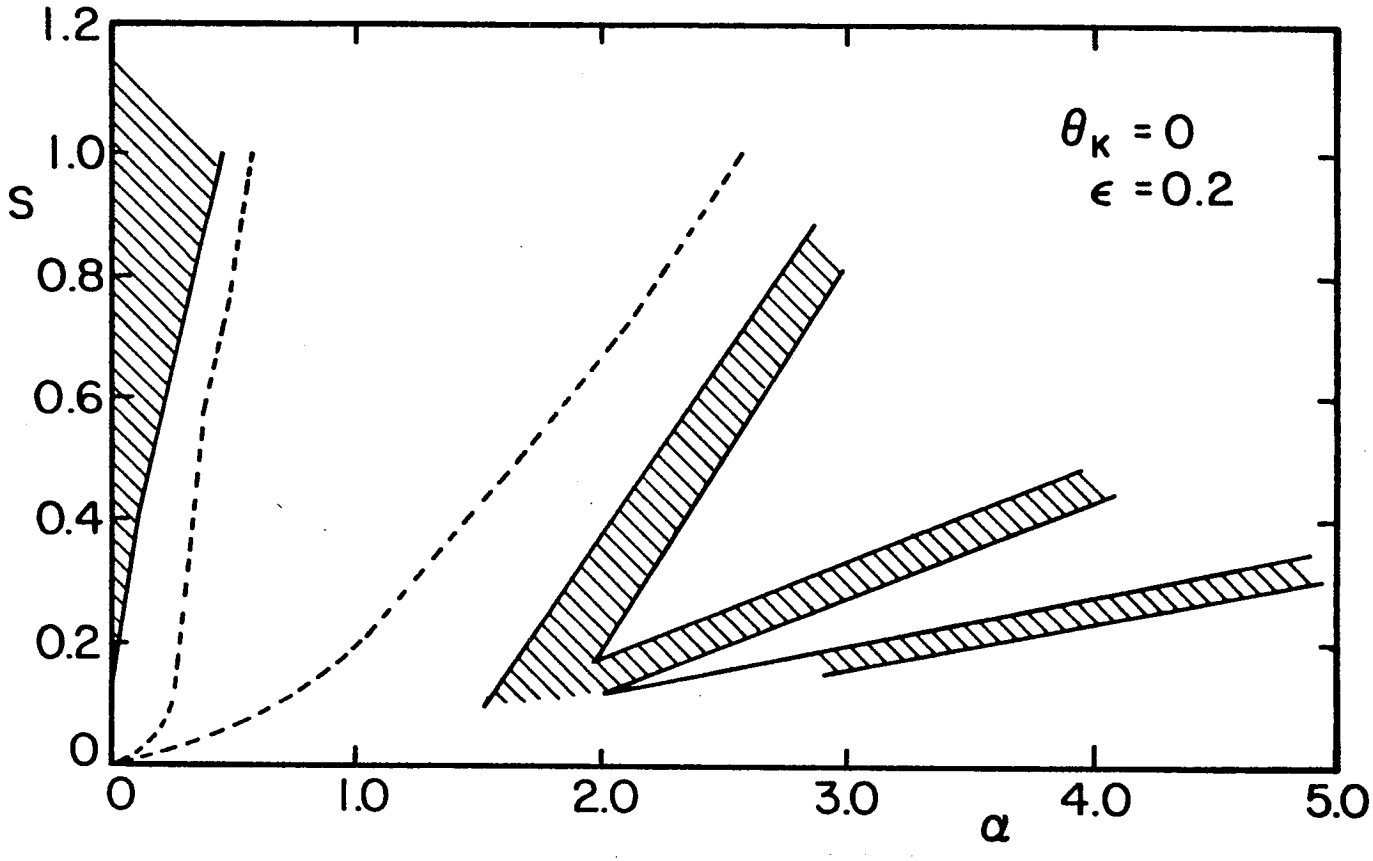

Fig. 10

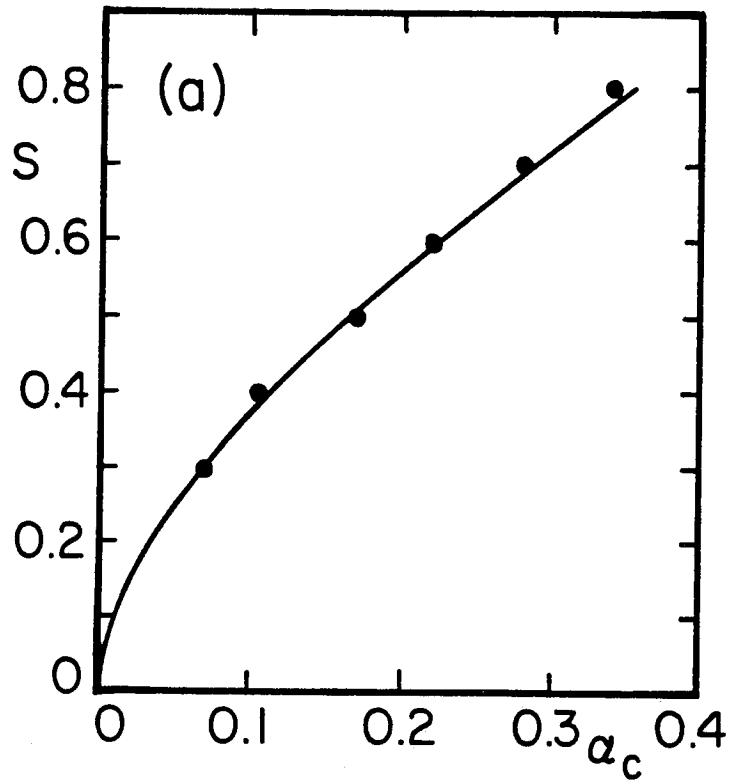

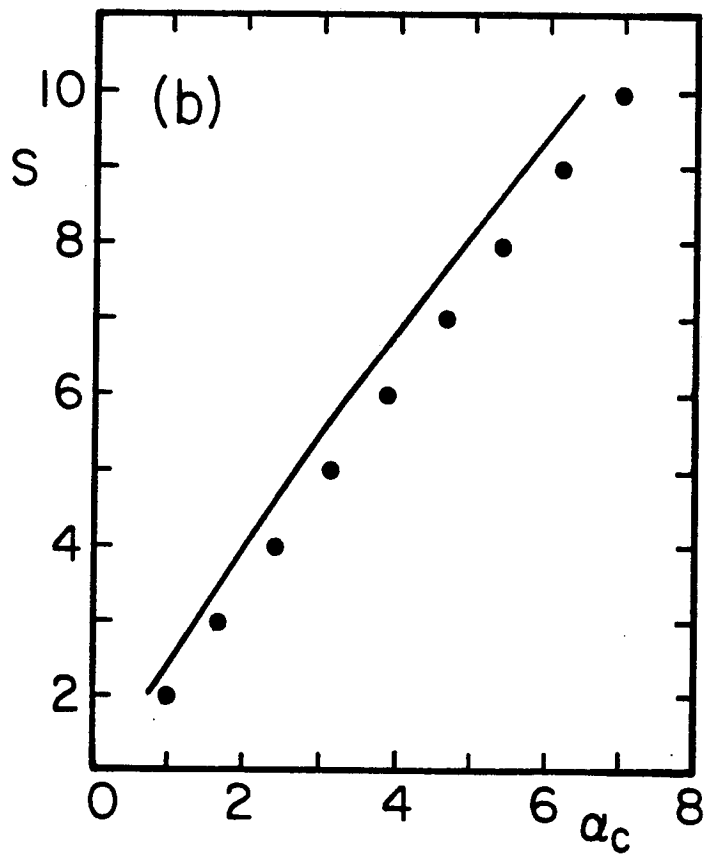

Fig. 11

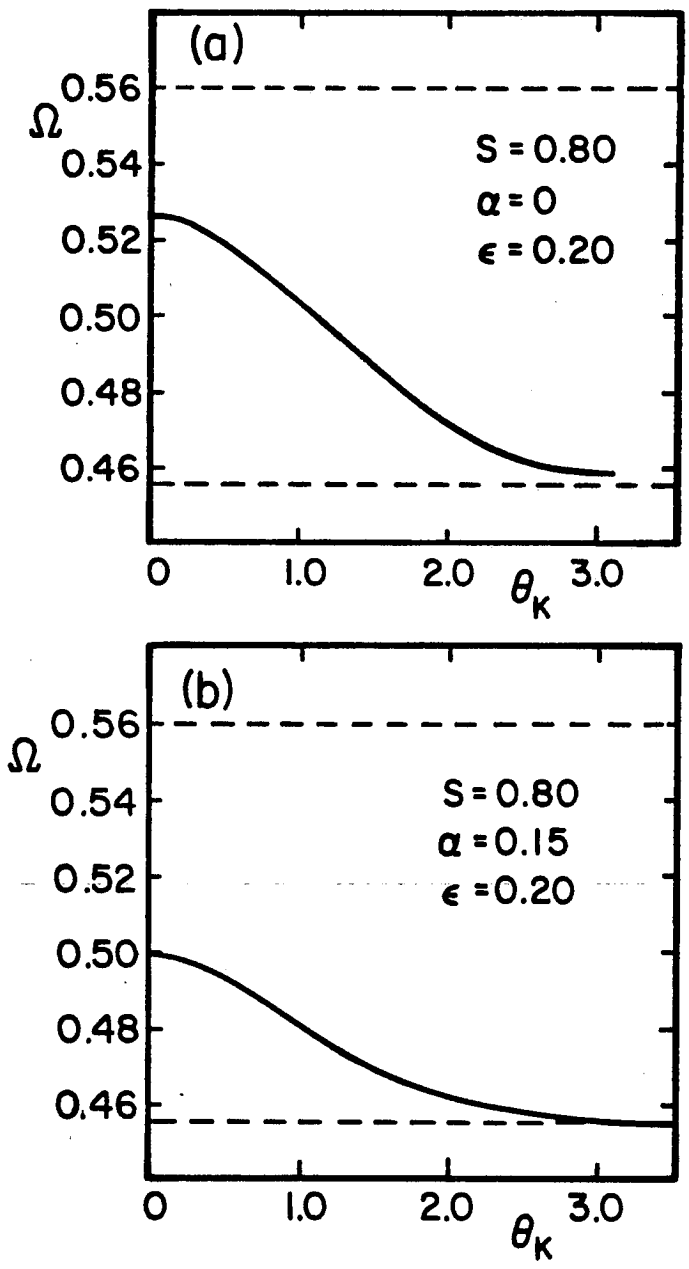
(a)
Ω
0.56
0.54
0.52
0.50
0.48
0.46
S = 0.80
α = 0
ϵ = 0.20
0
1.0
2.0
3.0
θK
(b)
Ω
0.56
0.54
0.52
0.50
0.48
0.46
S = 0.80
α = 0.15
ϵ = 0.20
0
1.0
2.0
3.0
θK

Fig. 12

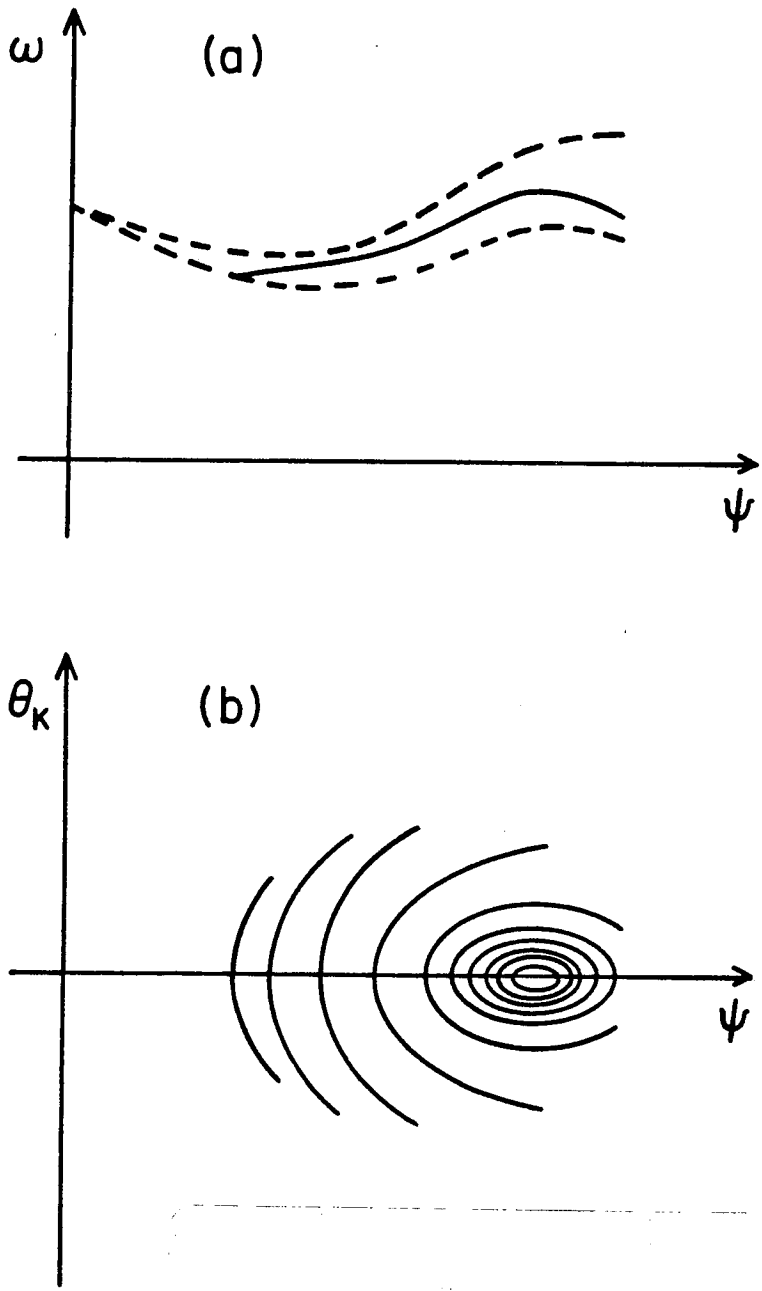

Fig. 13

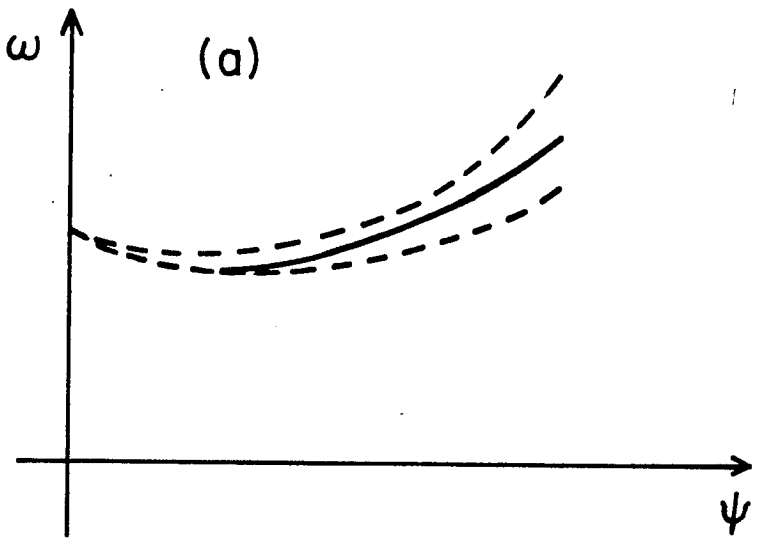

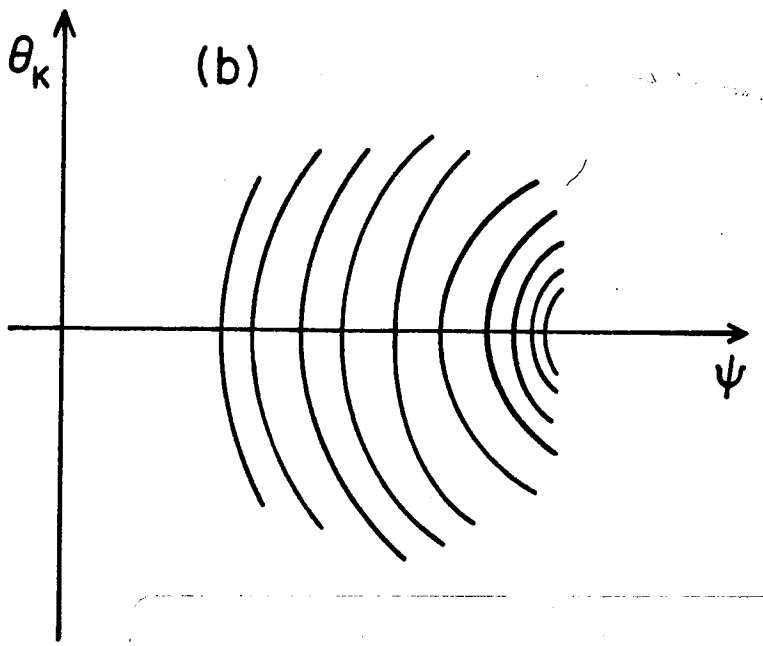

Fig. 14